Aust. J. Phys., 1990, **43**, 9–17

Which Potentials have to be Surface Peaked to Reproduce Large Angle Proton Scattering at High Energy?

Jacques Raynal

School of Physics, University of Melbourne,
Parkville, Vic. 3052, Australia.
Permanent address: Service de Physique Théorique de Saclay,
F-91191 Gif-sur-Yvette Cedex, France.

Abstract

Corrections to the usual form factors of the optical potential are studied with a view to getting a better fit for proton elastic scattering at large angles on ^{40}Ca at 497 and 800 MeV. When a real surface form factor is added to the central potential in the Schrödinger formalism, the experimental data are as well reproduced as in the standard Dirac formalism. Coupling to the strong 3^- collective state gives a better fit. The use of surface corrections to the imaginary Dirac potential also gives improved results. A slightly better fit is obtained by coupling to the 3^- state with, at the same time, a weakening of these corrections. Further corrections to the potential do not give significant improvements.

1. Introduction

In recent articles (Shim *et al.* 1988; Cooper 1989) it has been suggested that the form factor of the imaginary potentials used in the Dirac phenomenology of elastic nucleon scattering should contain a volume plus a surface term to fit large angle data. Up to now, the advantage of Dirac phenomenology comes primarily from the results obtained with pure volume potentials. If we add surface terms this advantage has to be reexamined by comparison with nonrelativistic calculations which also include some surface terms. Furthermore, the coupling to a strong collective state such as the 3^- at 3·74 MeV in ^{40}Ca also gives a better fit for these data (Raynal 1987) and it is of some interest to see if these surface corrections persist or are damped by this coupling.

2. Dirac versus Schrödinger Formalism

The Dirac equation used to describe scattering of nucleons by nuclei ($c = 1$):

$$\left(\frac{\hbar}{\mathrm{i}}\,\boldsymbol{\alpha}\cdot\nabla+\beta\{m+V_{\mathrm{S}}(r)\}+V_{\mathrm{V}}(r)+\frac{\mathrm{i}\,\hbar}{2m}\beta\boldsymbol{\alpha}\cdot\{\nabla V_{\mathrm{T}}(r)\}\right)\psi(r)=E\psi(r), \tag{1}$$

where $V_{\mathrm{S}}(r)$, $V_{\mathrm{V}}(r)$ and $V_{\mathrm{T}}(r)$ are three complex potentials, can be replaced by the Schrödinger equation:

$$\{\nabla^2-V_1(r)-\mathrm{i}\,\boldsymbol{\sigma}\cdot\nabla V_2(r)\times\nabla+k^2\}f(r)=0, \tag{2}$$

0004-9506/90/010009$03.00

where

$$V_1(r) = \tfrac{3}{4}\left(\frac{\nabla \mathcal{D}(r)}{\mathcal{D}(r)}\right)^2 - \frac{\nabla^2 \mathcal{D}(r)}{2\mathcal{D}(r)}$$

$$+ \frac{1}{\hbar^2}\{2mV_s(r) + 2EV_v(r) + V_s^2(r) - V_v^2(r)\}, \tag{3}$$

$$V_2 = \ln \mathcal{D}(r), \tag{4}$$

$$\mathcal{D}(r) = D(r)\exp\{V_T(r)/m\}, \tag{5}$$

$$D(r) = E + m - V_v(r) + V_s(r), \tag{6}$$

but where the wavefunction $f(r)$ is given in terms of the large components $F(r)$ of the Dirac equation by

$$f(r) = D(r)^{-\frac{1}{2}}F(r). \tag{7}$$

This derivation takes into account the possible anisotropy of all the potentials; the tensor potential is written in such a way that it includes the Coulomb potential multiplied by the anomalous magnetic moment if one wants to take it into account: therefore, it differs from the one of Clark *et al.* (1985) which was the monopole part of the tensor potential used here. The spin–orbit potential appears in a form used for a long time for nucleon inelastic scattering (Sherif and Blair 1968; Sherif 1968). If the potentials are allowed to have any radial dependence, the only difference between Dirac phenomenology and the earlier one appears in inelastic scattering: in the coupled Schrödinger equations, the part of $D(r)$ which acts between different levels is neglected in equation (7). [For example, in the first order vibrational model, the boson operators of $D(r)$ are neglected.] With a spin-zero target, the difference turns out to be negligible (Raynal and Sherif 1986). The real part of the potential (3) presents a 'wine-bottle-bottom' shape (Arnold *et al.* 1981), that is, the same mixture of volume and surface terms advocated for the Dirac imaginary potentials. The Coulomb potential, even without a tensor potential, generates a long range term in r^{-3} in the spin–orbit potential (4) which is the Mott–Schwinger interaction necessary to describe the polarisation of neutron elastic scattering (Guss *et al.* 1985) and which must be included in the nonrelativistic optical model. There is also in the central potential (3) a long range term in r^{-2} coming from the square of the Coulomb potential, not justified in the nonrelativistic optical model and without notable effects. As long as only the elastic scattering is taken into account, there is no difference between Dirac and Schrödinger equations if the potentials are allowed to have any form factor and restricted only to be of finite range.

In the following, we quote as Dirac calculations the ones in which $V_s(r)$ and $V_v(r)$ are parametrised in terms of Woods–Saxon form factors and their derivatives; the coupled equations are solved as already described (Raynal 1987). We quote as Schrödinger calculations the ones in which $V_1(r)$ and $V_2(r)$

are parametrised and the coupled equations solved in the usual way. The same kinematics are used in the two cases.

3. Analysis of the Different Corrections

To see for which potentials a surface term is necessary, let us consider data for elastic proton scattering on ^{40}Ca at 497 MeV (Hoffmann *et al.* 1981, 1988; Rahbar *et al.* 1981; Seth *et al.* 1985) and at 800 MeV (Blesynski *et al.* 1982; Fergerson *et al.* 1986). Data for the cross sections are available up to a large momentum transfer; data for polarisation have been measured up to the same angle at 497 MeV but not so far at 800 MeV; data for Q are available only for smaller angles. All these data are taken into account, even if two different measurements are given at the same angle; to overcome the large contribution of the cross section in the total χ^2, the contribution of the polarisation is multiplied by 5 and the contribution of Q is multiplied by 10. Data on the inelastic cross section and analysing power for the 3^- state at 3·74 MeV are known; in coupled channels calculations, they are not introduced in the χ^2 but used to show the prediction with the same deformation parameter $\beta = 0{\cdot}39$ for all the potentials. Such a coupling to the 3^- state gives a better fit to the backward angles (Raynal *et al.* 1989); we want to see what happens to the surface terms which are introduced in the potential in order to achieve the same goal. One has to remember that other collective states can also have a contribution. In the calculations presented here, the reduced mass is used and the charge is assumed to be a homogeneous sphere with the same radius as the volume real vector potential in the Dirac formalism or of the reduced value 1·05 fm in the Schrödinger formalism.

In the Dirac phenomenology there is a large ambiguity between the imaginary parts of the scalar and the vector potential (Raynal 1987). The imaginary part of the scalar potential can be suppressed (De Swiniarski *et al.* 1988), at least when the large angle data are not known. Five searches on all the parameters have been done: this 9-parameter Dirac potential, the usual 12-parameter Dirac potential, adding tensor potentials, adding surface terms to the imaginary potentials and adding surface terms to both real and imaginary potentials. These searches were done for elastic scattering only and with the coupling to the 3^- state. With tensor potentials, the fits are slightly better than with the addition of imaginary surface potentials, but the parameters are unrealistic, very different without and with coupling. The optical model parameters of the other searches are given in Table 1 and the results of the 9-parameter Dirac potential are shown by the dot–dash curves in Fig. 1. As seen in Table 1, at 497 MeV, with the coupling to the 3^- state, the 9-parameter Dirac potential gives better results than the plain 12-parameter one, except for Q; at 800 MeV, results are similar for the cross section and polarisation. Coupled channels results at 497 MeV with the 12-parameter Dirac potential are shown by the solid curves in Fig. 1. These results are slightly better than the no-coupling results with surface imaginary potentials at 497 MeV, but not at 800 MeV. However, coupling to the 3^- state improves the fits at the two energies; it decreases the imaginary surface potentials by a factor greater than 2 at 497 MeV where they are very peaked; at 800 MeV it suppresses the vector one, but these form factors are broad and all the parameters of

Table 1. Optical parameters for the Dirac equation at 497 MeV (upper part) and 800 MeV (lower part)

Values given on the same line as the χ^2 are those of a Woods–Saxon potential; the others are those of a derivative of a Woods–Saxon potential normalised to a unit maximum value. In each case, results obtained with the coupling to the first 3^- state at 3·74 MeV with $\beta = 0·39$ are given below those of the elastic scattering calculation. The charge is a uniform sphere with the radius of the real part of the vector potential

Scalar potential						Vector potential						χ^2 per point		
Real part			Imaginary part			Real part			Imaginary part					
V	r	a	V	r	a	V	r	a	V	r	a	σ	P	Q
−281·9	1·049	0·688				198·7	1·038	0·642	−43·3	1·060	0·600	27·94	7·99	9·53
−262·1	1·078	0·664				186·4	1·064	0·622	−38·4	1·094	0·579	11·80	5·39	7·08
−324·9	1·033	0·668	47·0	1·152	0·500	217·3	1·035	0·629	−67·8	1·120	0·540	22·28	5·39	3·56
−295·4	1·062	0·657	39·4	1·154	0·510	201·0	1·058	0·622	−61·5	1·124	0·541	7·99	3·75	3·30
−297·9	1·050	0·657	68·2	0·971	0·871	199·3	1·053	0·614	−75·6	1·050	0·710	11·47	3·84	3·14
			2·05	1·118	0·286				−1·42	1·121	0·247			
−286·1	1·070	0·654	33·4	1·118	0·826	194·2	1·069	0·613	−56·1	1·105	0·672	7·18	2·68	1·75
			1·00	1·116	0·328				−0·50	1·129	0·192			
−296·8	1·067	0·623	50·6	0·997	0·848	182·9	1·056	0·618	−62·4	1·076	0·675	7·66	3·19	3·05
−1·33	1·396	0·653	2·66	1·128	0·320	7·62	0·930	0·571	−1·95	1·113	0·301			
−258·8	1·079	0·589	24·2	1·167	0·794	179·0	1·080	0·595	−47·1	1·140	0·636	5·33	2·45	2·45
−7·19	1·211	0·708	1·23	1·169	0·340	5·43	0·890	0·590	−0·25	1·193	0·232			
−298·6	1·003	0·750				181·5	1·004	0·688	−63·5	1·023	0·629	35·99	4·13	9·51
−265·1	1·053	0·713				161·6	1·053	0·658	−53·9	1·069	0·600	22·38	4·25	7·51
−351·6	0·978	0·735	75·4	1·065	0·616	196·3	0·994	0·690	−102·0	1·048	0·612	25·23	3·37	2·64
−307·4	1·030	0·707	61·8	1·095	0·604	174·5	1·039	0·668	−87·6	1·080	0·593	12·86	3·81	2·86
−267·1	1·042	0·688	173·6	0·743	0·494	147·3	1·054	0·648	−152·0	0·809	0·538	8·24	1·89	1·87
			29·7	0·961	0·601				−27·7	0·989	0·601			
−263·9	1·058	0·681	122·7	0·801	0·550	151·4	1·059	0·652	−114·0	1·009	0·603	6·80	1·86	2·82
			24·4	0·989	0·611				−2·0	1·156	0·487			
−219·0	1·174	0·616	114·3	0·781	0·613	125·3	0·965	0·555	−115·0	0·869	0·600	5·24	1·88	1·48
18·9	1·161	0·564	5·5	1·229	0·420	28·6	1·021	0·617	−11·3	1·063	0·531			
−223·5	1·036	0·672	68·8	0·845	0·571	131·9	1·085	0·694	−80·8	1·023	0·579	5·58	1·90	1·69
−24·4	1·013	0·577	9·5	1·065	0·489	6·9	0·944	0·707	−3·9	1·133	0·473			

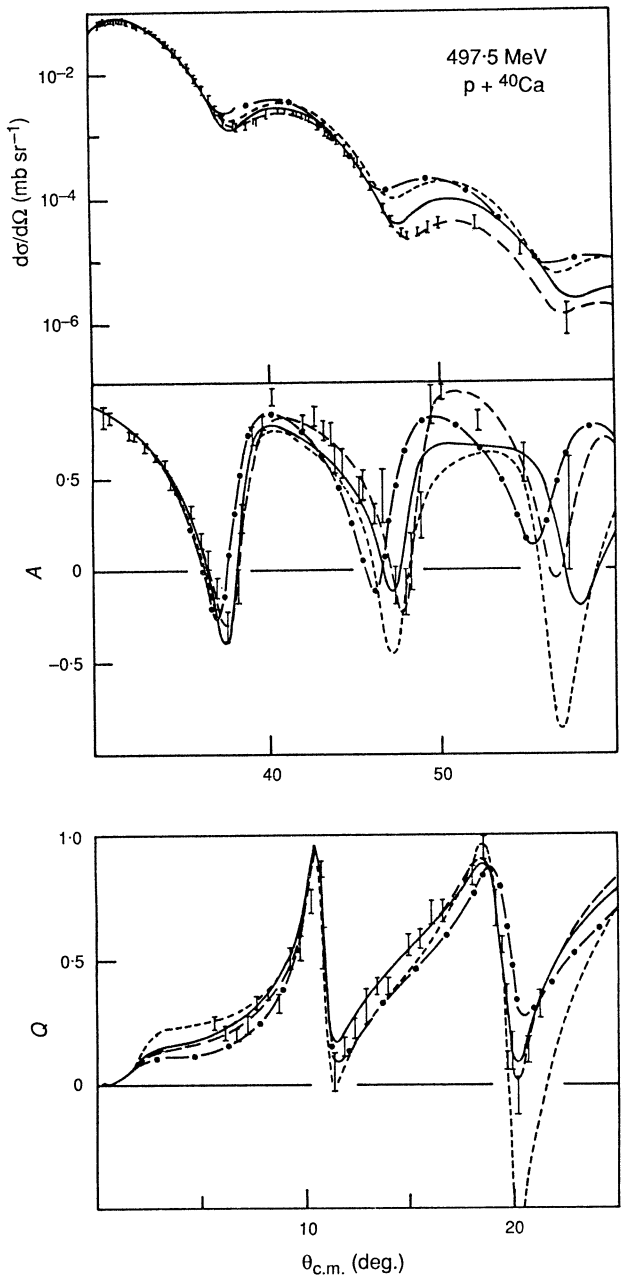

Fig. 1. Cross section, polarisation and Q parameter at 497 MeV. The short-dash curves are obtained with the 12-parameter Schrödinger equation and the dot–dash ones with the 9-parameter Dirac equation. The solid curves are the results obtained with the 12-parameter Dirac equation including the coupling to the 3^- state. The long-dash curves are obtained with the 24-parameter Schrödinger equation including the coupling to the 3^- state: the total χ^2 is only 1% larger than the best result obtained with the Dirac equation.

Table 2. Optical parameters for the Schrödinger equation at 497 MeV (upper part) and 800 MeV (lower part)

Same presentation as for Table 1. The charge is a uniform sphere of reduced radius 10·5 fm

Central potential						Spin–orbit potential						χ^2 per point		
Real part			Imaginary part			Real part			Imaginary part					
V	r	a	V	r	a	V	r	a	V	r	a	σ	P	Q
11·39	1·101	0·475	44·97	1·044	0·544	0·84	1·216	0·734	−1·83	0·939	0·595	22·70	6·42	11·92
9·62	1·135	0·515	43·82	1·060	0·527	0·82	1·211	0·718	−2·06	0·912	0·621	15·03	5·29	16·02
−10·82	1·272	0·418	45·53	1·042	0·557	1·81	0·999	0·755	−0·98	1·005	0·585	21·50	4·10	5·94
8·07	1·109	0·560												
−17·87	1·250	0·465	42·72	1·065	0·555	1·71	1·032	0·686	−0·68	1·068	0·506	8·20	3·19	3·84
11·24	1·093	0·596												
−28·75	1·338	0·576	34·02	1·118	0·596	1·62	1·057	0·583	−0·30	0·787	0·383	7·39	4·49	2·73
18·57	1·174	0·663							−0·11	1·024	0·529			
−27·24	1·298	0·638	37·68	1·092	0·586	1·66	1·057	0·611	−0·31	0·846	0·346	5·04	3·35	2·77
15·97	1·158	0·707							−0·17	0·999	0·506			
−22·91	1·298	0·508	36·37	1·065	0·538	1·54	1·055	0·625	−0·49	0·816	0·428	6·41	3·03	2·35
14·57	1·144	0·605	0·36	1·409	0·408	0·036	0·898	0·306	−0·19	0·995	0·498			
−24·60	1·278	0·546	36·42	1·101	0·542	1·57	1·065	0·615	−0·37	0·900	0·448	4·83	2·66	2·32
14·34	1·138	0·643	0·35	1·396	0·448	0·018	0·851	0·355	−0·13	1·027	0·486			
−9·32	0·961	0·513	71·31	1·018	0·595	1·31	0·957	0·800	−1·14	0·898	0·689	30·43	5·16	7·42
14·32	0·934	0·567	61·77	1·062	0·569	1·19	1·007	0·756	−0·72	1·017	0·603	24·85	5·89	5·69
−27·11	1·258	0·483	62·45	1·040	0·603	1·27	0·994	0·697	−0·45	1·025	0·607	13·55	4·42	2·51
13·89	1·110	0·576												
−29·39	1·250	0·533	58·40	1·064	0·587	1·03	1·070	0·632	−0·31	1·101	0·491	8·66	3·51	1·93
14·02	1·098	0·641												
−26·47	1·267	0·508	61·71	1·039	0·607	1·04	1·043	0·653	−0·67	0·844	0·663	8·90	2·04	1·67
13·41	1·121	0·602							−0·03	1·057	0·429			
−27·94	1·247	0·524	57·27	1·064	0·593	0·92	1·089	0·615	−0·53	0·828	0·595	7·22	2·05	1·50
12·54	1·111	0·629							−0·06	1·040	0·484			
−22·16	1·279	0·530	68·81	1·032	0·601	0·89	1·074	0·568	−0·76	0·777	0·548	6·49	2·07	1·55
11·49	1·129	0·631	−3·22	0·812	0·641	−0·11	1·095	0·519	−0·11	0·998	0·523			
−19·74	1·263	0·481	70·54	1·042	0·585	0·95	1·256	0·716	−0·75	0·782	0·558	6·05	1·75	1·57
9·43	1·117	0·604	−4·67	0·855	0·531	−0·17	1·223	0·698	−0·12	0·988	0·529			

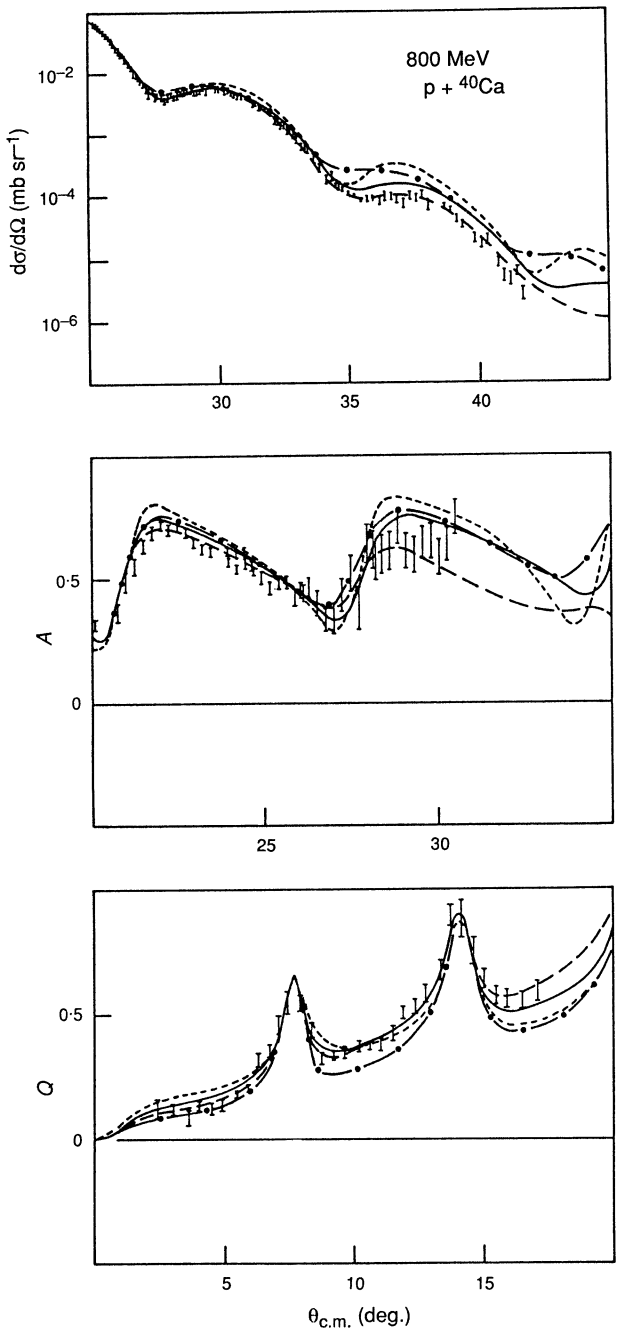

Fig. 2. Cross section, polarisation and Q parameter at 800 MeV. The short-dash and dot–dash curves are as in Fig. 1. The solid curves are the results obtained with the 15-parameter Schrödinger equation (with surface real potential) including the coupling to the 3^- state. The long-dash curves are obtained with the 24-parameter Dirac equation without coupling to the 3^- state: the total χ^2 is 4·8% smaller than that obtained with coupling and 3·3% smaller than the best result obtained with the Schrödinger equation.

the imaginary potentials are significantly changed. With real and imaginary surface potentials, the fits are very good with and without coupling to the 3^- state but the inelastic analysing power gets considerably worse than in all other cases.

Five searches on all the parameters have been done with the Schrödinger equation: the usual 12-parameter volume optical potential, adding a surface real central potential, adding a complex central potential, adding a surface real central potential and an imaginary spin–orbit potential, and adding surface potentials everywhere. A complex surface central potential does not improve the fits obtained with a real one: its imaginary part vanishes by getting too small a radius and diffuseness at 497 MeV and stays small at 800 MeV. Results of all the other searches are given in Table 2. Here also, coupling to the 3^- state improves the fits in all cases; the inelastic analysing power is quite good except when surface potentials are added everywhere. Results of the usual 12-parameter Schrödinger potential are given by the short-dash curves in both Figs 1 and 2; coupled channels with a surface real central potential at 800 MeV are given by the solid curves in Fig. 2.

4. Conclusions

In conclusion the 9-parameter Dirac potentials and 12-parameter Schrödinger potentials are quite similar. This does not contradict De Swiniarski *et al.* (1988) where no large angle data were taken into account. There is also a rough equivalence between 12-parameter Dirac potentials and 15-parameter Schrödinger potentials (with addition of a surface real potential) and also between the 18-parameter potentials (two imaginary surface potentials in Dirac phenomenology or surface real central and imaginary spin–orbit potentials with Schrödinger equation). In the Dirac phenomenology, the coupling to the 3^- state decreases the imaginary surface potentials and gives a change of sign for the real scalar surface potential at 800 MeV: so, the imaginary surface potential appears as a correction to the absence of coupling and the real surface potential appears more as an unjustified random result. In the Schrödinger phenomenology, the surface potentials are more stable with respect to the coupling. In all these cases, the coupling to the 3^- state improves the fit except for a $4 \cdot 8\%$ increase of the total χ^2 with the 24-parameter Dirac equation at 800 MeV. With this coupling and the optical potential obtained with the elastic scattering, χ^2 increases strongly for small scattering angles (not shown in the figures). The use of 24 parameters always gives a very poor inelastic analysing power; at 497 MeV, all the other calculations give fair agreement for the inelastic scattering with a ratio of 2 between the maximum and the minimum χ^2 for the cross section and for the analysing power; at 800 MeV, the backwards inelastic scattering is not reproduced and the χ^2 are more spread, but the small angle scattering is well reproduced. Attempts to use the Dirac equations with only one imaginary volume plus surface form factor failed. Some calculations done with coupling to the 3^- and 2^+ states gave slightly better results. It is not certain that the coupling to the 3^- state at $3 \cdot 74$ MeV accounts for all the second order collective effects. So, it is not reasonable to obtain a very good fit to the scattering at large angles at the price of too many parameters. For these reasons, it seems reasonable to use

the 12-parameter Dirac potential or the 15-parameter Schrödinger potential; their results, including the coupling to the 3^- state, are shown by the solid curves in the figures at 497 and 800 MeV respectively. The best results with 24-parameter potentials are given by the long-dash curves to show that equivalent results can be obtained with both formalisms.

Acknowledgments

The author thanks Prof. H. S. Sherif and Dr Ken Amos for helpful discussions and E. D. Cooper for the communication of his preprint.

References

Arnold, L. G., Clark, B. C., Mercer, R. L., and Schwandt, P. (1981). *Phys. Rev.* C **23**, 1949.
Blesynski, E., *et al.* (1982). *Phys. Rev.* C **25**, 2563.
Clark, B. C., Hama, S., Kälbermann, S. G., Cooper, E. D., and Mercer, R. L. (1985). *Phys. Rev.* C **31**, 694.
Cooper, E. D. (1989). *Nucl. Phys.* A **495**, 483.
De Swiniarski, R., Pham, D. L., and Raynal, J. (1988). *Phys. Lett.* B **213**, 247.
Fergerson, R. W., *et al.* (1986). *Phys. Rev.* C **33**, 239.
Guss, P. P., Byrd, R. C., Floyd, C. E., Howell, C. R., Murphy, K., Tungate, G., Pedroni, R. S., Walter, R. L., Delaroche, J. P., and Clegg, T. B. (1985). *Nucl. Phys.* A **438**, 187.
Hoffmann, G. W., *et al.* (1981). *Phys. Rev. Lett.* **47**, 1436.
Hoffmann, G. W., *et al.* (1988). *Phys. Rev.* C **37**, 1307.
Rahbar, A., *et al.* (1981). *Phys. Rev. Lett.* **47**, 1811.
Raynal, J. (1987). *Phys. Lett.* B **196**, 7.
Raynal, J., and Sherif, H. S. (1986). *J. Phys. Soc. Jpn Suppl.* **55**, 924.
Raynal, J., Sherif, H. S., Kobos, A. M., Cooper, E. D., and Johansson, J. I. (1989). *Phys. Lett.* B **218**, 403.
Seth, K. K., *et al.* (1985). *Phys. Lett.* B **158**, 23.
Sherif, H. S. (1968). Spin-dependent effects in proton inelastic scattering. Thesis, Univ. of Washington.
Sherif, H., and Blair, J. S. (1968). *Phys. Lett.* B **26**, 489.
Shim, S., Clark, B. C., Hama, S., Cooper, E. D., Mercer, R. L., Ray, L., and Hoffmann, G. W. (1988). *Phys. Rev.* C **38**, 1968.

Manuscript received 7 August, accepted 6 December 1989